Appl Compos Mater (2006) 13: 345–367
DOI 10.1007/s10443-006-9021-z

Non-Local Theory Solution for an Anti-Plane Shear Permeable Crack in Functionally Graded Piezoelectric Materials

Zhen-Gong Zhou · Biao Wang

Received: 24 February 2006 / Accepted: 1 June 2006 /
Published online: 8 September 2006

Abstract In this paper, the non-local theory solution of a Griffith crack in functionally graded piezoelectric materials under the anti-plane shear loading is obtained for the permeable electric boundary conditions, in which the material properties vary exponentially with coordinate parallel to the crack. The present problem can be solved by using the Fourier transform and the technique of dual integral equation, in which the unknown variable is the jump of displacement across the crack surfaces, not the dislocation density function. To solve the dual integral equations, the jump of the displacement across the crack surfaces is directly expanded in a series of Jacobi polynomials. From the solution of the present paper, it is found that no stress and electric displacement singularities are present near the crack tips. The stress fields are finite near the crack tips, thus allows us to use the maximum stress as a fracture criterion. The finite stresses and the electric displacements at the crack tips depend on the crack length, the functionally graded parameter and the lattice parameter of the materials, respectively. On the other hand, the angular variations of the strain energy density function are examined to associate their stationary value with locations of possible fracture initiation.

Key words crack · functionally graded piezoelectric materials · mechanics of solids · non-local theory

1 Introduction

Electromechanical coupling effects for piezoelectric materials have been known for sometimes. However, only in recent years much interest has been generated because of their application of electronic devices, such as actuators and sensors. Concern for reliability and durability of these devices necessitates a fundamental understanding of the damage and

Z.-G. Zhou (✉)
Center for Composite Materials, Harbin Institute of Technology,
P.O. Box 1247, Harbin 150001, People's Republic of China
e-mail: zhouzhg@hit.edu.cn

B. Wang
School of Physics and Engineering, Sun Yat-Sen University, Guangzhou 510275, China

fracture process of piezoelectric ceramics. This has led to a host of research findings [1–8] on the fracture mechanics of piezoelectric materials. On the other hand, the development of functionally graded materials (FGMs) has demonstrated that they have the potential to reduce the stress concentration and increase of fracture toughness. Consequently, the concept of FGMs was be extended to the piezoelectric materials to improve the reliability of piezoelectric materials and structures. Some applications of functionally graded piezoelectric materials (FGPMs) have been made as shown in [9]. Recently, the fracture problems of (FGPMs) have been studied in [10–15]. To our knowledge, Li and Weng [15] first applied the concept of fracture mechanics on a finite crack in a strip of functionally graded piezoelectric material. They found that the singular stresses and the singular electric displacements at the crack tips in FGPMs carry the same forms as those in the homogeneous piezoelectric materials but the magnitudes of the intensity factors are dependent on the gradient of the FGPM properties. In the theoretical studies of crack problems in piezoelectric materials, the researchers assume the crack surfaces to be stress-free, but they have different opinions about the electrical boundary condition at the crack surfaces. Since the dielectric constant of air or the medium between the crack faces is very small compared to that of the piezoelectric materials, Deeg [16] and Pak [17] have assumed crack surfaces to be free of surface charge. This is the impermeable crack mode. According to this crack mode, the interaction of multiple parallel impermeable cracks in the piezoelectric materials was studied by the 'pseudo-traction-electric displacement' method in [18]. On the other hand, some authors as Parton [19], Mikhailov and Parton [20] considered that the thickness of the crack is very small and cracks in a piezoelectric material consist of vacuum, air or some other gas. So the electric potential and the electric displacement should be continuous across the crack surfaces. This is the permeable crack mode. Along this line, the crack problem in piezoelectric materials was studied in [6]. Using the analogy of a capacitor filled by a medium, Hao and Shen [21] used a boundary condition in which the electrical permeability of air in the crack gas was considered. It is interesting to note that very different results were obtained by changing the boundary conditions [22]. However, these solutions [10–26] *contain the theoretical stress and the theoretical electric displacement* singularities at the crack tips. *In fact, the stress fields and the electric displacement fields at the crack tips should be finite.* As a result of this, beginning with Griffith, all fracture criteria in use today based on other considerations, e.g., energy, the *J*-integral [27] and the strain gradient theory [28]. Now the main difficulty is remained ambiguous how to provide effective fracture criteria for functionally graded piezoelectric materials.

To overcome the *theoretical* stress singularities at the crack tips in the classical elastic fracture theory, Eringen et al. [29–31] used the non-local theory to discuss the stresses near the tips of a sharp line crack in an isotropic elastic plate subject to uniform tension, shear and anti-plane shear, and the resulting solutions did not contain any stress singularities at the crack tips. This allows us to use the maximum stress as a fracture criterion. In contrast to these local approaches, of zero-range internal interactions, the modern non-local continuum mechanics originated and developed in the last five decades. Edelen [32] contributed some mathematical formalism while Green and Rivilin [33] simply enunciated some postulates for the non-local theory. On the other hand, Eringen [34] contributed not just the complete physics and mathematics of the non-local theory but also, in addition, shaped the theory into a concrete form making it viable for practical applications to boundary value problems. According to the non-local theory, the stress at a point X in a body depends not only on the strain at point X but also on that at all other points of the body. This is contrary to the classical theory that the stress at a point X in a body depends only on the strain at point X. In [35], the basic theory of non-local elasticity was stated with emphasis on the

difference between the non-local theory and the classical continuum mechanics. Other results have been given by the application of the non-local elasticity to the fields such as a dislocation near a crack [36, 37] and fracture mechanics problems [38, 39]. The results of those concrete problems that were solved display a rather remarkable agreement with experimental evidence. This can be used to predict the cohesive stress for various materials and the results close to those obtained in atomic lattice dynamics [40, 41]. To our knowledge, Zhou et al. [42–45] first applied the concept of the non-local theory on a finite crack in the piezoelectric materials. They found that no stress and electric displacement singularities are present at the crack tips in the piezoelectric materials. Recently, some static and dynamic fracture problems [46–50] in an isotropic elastic material, the anisotropic elasticity materials, the functionally graded materials and the functionally graded piezoelectric material have been investigated by use of the non-local theory. The traditional concept of linear elastic fracture mechanics and the non-local theory are extended to include the functionally graded piezoelectric materials. However, the materials variation directions in [49, 50] are all vertical to the crack. To our knowledge, the non-local theory solution of a crack in the functionally graded piezoelectric materials has not been studied, in which the shear modulus, the piezoelectric coefficient and the dielectric parameter vary exponentially with coordinate parallel to the crack. Thus, the present work is an attempt to fill this information needed. Here, we just attempt to give a theoretical solution for this problem.

In the present paper, the non-local solution of a permeable crack subjected to anti-plane shear in functionally graded piezoelectric materials was studied. Here, it is assumed that the material properties vary exponentially with coordinate parallel to the crack. This is different from the [49, 50]. Through the Fourier transform, the problem of the present paper is reduced to a pair of dual integral equations, in which the unknown variable is the jump of the displacement across the crack surfaces, *not the dislocation density function*. To solve the dual integral equations, the jump of the displacement across the crack surfaces is directly expanded in a series of Jacobi polynomials and the Schmidt method [51] is used. *From the solution of the present paper, it can be obtained that the stress field and the electric field do not contain singularities near the crack tips*. The stress field and the electric field for the non-local theory are similar to that of the classical elasticity solution away from the crack tips. Near the crack tips, the stress and the electric displacement fields depend on the lattice parameter and the functionally graded parameter. The angular variations of the strain energy density function are also examined to associate their stationary value with locations of possible fracture initiation.

2 The Crack Model

Consider an infinite functionally graded piezoelectric material plane containing a Griffith permeable crack of length $2l$ along the x-axis. The piezoelectric boundary-value problem for anti-plane shear is considerably simplified if we consider only the out-of-plane displacement and the in-plane electric displacement fields as shown in Figure 1. *As discussed in* [22], *the permeable electric boundary condition will be enforced in the present study*, i.e., both the electric potential and the normal electric displacement are assumed to be continuous across the crack surfaces. So the external electric displacement D_0 need not to be considered in the present paper. It is assumed that the plate was only subjected to an anti-plane shear stress loading $\tau_{yz} = -\tau_0(x)$ ($-\tau_0(x)$ is the magnitude of the anti-plane shear stress loading.). Here, the standard superposition technique is used and only the perturbation

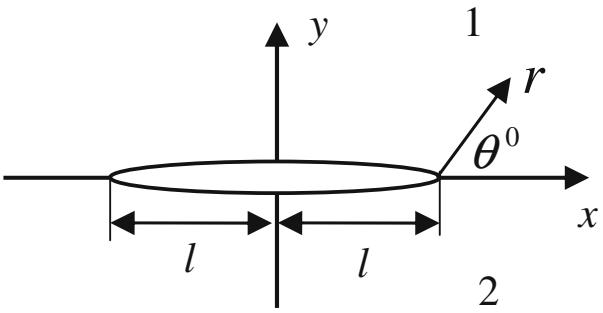

Figure 1 Crack in the FGPMs under anti-plane shear

fields are considered in the present paper. So the boundary conditions of the present problem are:

$$\tau_{yz}^{(1)}(x,0^+) = \tau_{yz}^{(2)}(x,0^-) = -\tau_0(x), |x| \le l \tag{1}$$

$$D_y^{(1)}(x,0^+) = D_y^{(2)}(x,0^-),\ \phi^{(1)}(x,0^+) = \phi^{(2)}(x,0^-),\ |x| \le \infty \tag{2}$$

$$\tau_{yz}^{(1)}(x,0^+) = \tau_{yz}^{(2)}(x,0^-),\ w^{(1)}(x,0^+) = w^{(2)}(x,0^-) = 0, |x| > l \tag{3}$$

$$w^{(i)}(x,y) = \phi^{(i)}(x,y) = 0,\ \text{for}\ \left(x^2+y^2\right)^{1/2} \to \infty, (i = 1,\ 2) \tag{4}$$

where $w^{(i)}$ (x, y) and $\phi^{(i)}$ (x, y) $(i = 1, 2)$are the mechanical displacement and the electric potential, respectively. $\tau_{zk}^{(i)}(x,y)$ and $D_k^{(i)}(x,y)$ $(k = x, y, i = 1, 2)$ are the anti-plane shear stress field and in-plane electric displacement field, respectively. Note that all quantities with superscript i $(i = 1, 2)$ refer to the upper half plane and the lower half plane. *In the present paper, it is a single-material fracture problem, not bi-materials*.

3 Basic Equations of Non-Local Functionally Graded Piezoelectric Materials

For the anti-plane shear problem, the basic equations of linear, isotropic, non-local functionally graded piezoelectric materials, with vanishing body force *and free charges* are [6, 8, 22]

$$\frac{\partial \tau_{xz}^{(i)}}{\partial x} + \frac{\partial \tau_{yz}^{(i)}}{\partial y} = 0 \tag{5}$$

$$\frac{\partial D_x^{(i)}}{\partial x} + \frac{\partial D_y^{(i)}}{\partial y} = 0 \tag{6}$$

$$\tau_{kz}^{(i)}(X) = \int_V \left[c'_{44}(|X'-X|)w_{,k}^{(i)}(X') + e'_{15}(|X'-X|)\phi_{,k}^{(i)}(X')\right]dV(X'), (k = x,y) \tag{7}$$

$$D_k^{(i)}(X) = \int_V \left[e'_{15}(|X'-X|)w_{,k}^{(i)}(X') - \varepsilon'_{11}(|X'-X|)\phi_{,k}^{(i)}(X')\right]dV(X'),\ (k = x,y) \tag{8}$$

where the only difference from the classical elastic theory and the piezoelectric theory is in the stress and the electric displacement constitutive Equations (3)–(4) in which the stress

$\tau_{zk}^{(i)}(x,y)$ and the electric displacement $D_k^{(i)}(x,y)$ at a point X not only depend on the $w_{,k}^{(j)}(X)$ and $\phi_{,k}^{(j)}(X)$, but also depend on the $w_{,k}^{(j)}(X)$ and $\phi_{,k}^{(j)}(X)$ at all the other points of the body. For isotropic functionally graded piezoelectric materials there exist only three material parameters, $c'_{44}(|X'-X|)$, $e'_{15}(|X'-X|)$ and $\varepsilon'_{11}(|X'-X|)$ which are functions of the distance $|X'-X|$. The integrals in Equations (3)–(4) are over the volume V of the body enclosed within a surface ∂V.

As discussed in [52, 53], it can be assumed in the form of $c'_{44}(|X'-X|)$, $e'_{15}(|X'-X|)$ and $\varepsilon'_{11}(|X'-X|)$ for which the dispersion curves of plane elastic waves coincide with those known in lattice dynamics. Among several possible curves the following has been found to be very useful

$$\left(c'_{44}(|X'-X|), e'_{15}(|X'-X|), \varepsilon'_{11}(|X'-X|)\right) = (c_{44}(x), e_{15}(x), \varepsilon_{11}(x))\alpha(|X'-X|) \quad (9)$$

$$\alpha(|X'-X|) = \alpha_0 \exp\left[-(\beta/a)^2(X'-X)(X'-X)\right] \quad (10)$$

where $\alpha(|X'-X|)$ is known as the influence function. β is a constant and can be determined by experiment. a is the characteristic length. The characteristic length may be selected according to the range and sensitivity of the physical phenomena. For instance, for the perfect crystals, a may be taken as the lattice parameter. For a granular material, a may be considered to be the average granular distance and for a fiber composite, the fiber distance, etc. In the present paper, a is taken as the lattice parameter. $c_{44}(x)$, $e_{15}(x)$ and $\varepsilon_{11}(x)$ are the shear modulus, piezoelectric coefficient and dielectric parameter of FGPMs, respectively. α_0 is determined by the normalization

$$\int_V \alpha(|X'-X|)dV(X') = 1 \quad (11)$$

Substituting Equation (10) into Equation (11), it can be obtained, in two-dimensional space,

$$\alpha_0 = \frac{1}{\pi}(\beta/a)^2 \quad (12)$$

Crack problems in the non-homogeneous piezoelectric materials do not appear to be analytically tractable for arbitrary variations of material properties. Usually, one tries to generate the forms of non-homogeneities for which the problem becomes tractable. Similar to the treatment of the crack problem for isotropic non-homogeneous materials in [10–15], we assume the material properties are described by:

$$c_{44}(x) = c_{440}\, e^{\gamma x},\ e_{15}(x) = e_{150}\, e^{\gamma x} \varepsilon_{11}(x) = \varepsilon_{110}\, e^{\gamma x} \quad (13)$$

where c_{440}, e_{150} and ε_{110} are the shear modulus, piezoelectric coefficient and dielectric parameter of FGPMs along $y = 0$, respectively. γ is the functionally graded parameter. $\gamma \neq 0$ is the case for the functionally graded piezoelectric materials. Here, the material variation direction is parallel to the crack. This is different from [49, 50]. When $\gamma = 0$, it will return to the homogenous piezoelectric material case in [44]. The expressions of Equation (13) are the purely mechanics assumptions.

Substitution of Equations (9)–(10) into Equations (7)–(8) yields

$$\tau_{kz}^{(i)}(X) = \int_V \alpha(|X' - X|)\sigma_{kz}^{(i)}(X')dV(X'), (k = x, y) \tag{14}$$

$$D_{kz}^{(i)}(X) = \int_V \alpha(|X' - X|)D_k^{c(i)}(X')dV(X'), (k = x, y) \tag{15}$$

where

$$\sigma_{kz}^{(i)} = e^{\gamma x}\left(c_{440}w_{,k}^{(i)} + e_{150}\phi_{,k}^{(i)}\right), (k = x, y) \tag{16}$$

$$D_k^{c(i)} = e^{\gamma x}\left(e_{150}w_{,k}^{(i)} - \varepsilon_{110}\phi_{,k}^{(i)}\right), (k = x, y) \tag{17}$$

The expressions (16)–(17) are the classical constitutive equations.

4 The Dual Integral Equation

Substituting Equations (14)–(15) into Equations (5)–(6), respectively, using Green-Gauss theorem, it can be obtained [29–31]:

$$\begin{aligned} & e^{\gamma x}\iint_V \alpha(|x' - x|, |y' - y|)\left\{c_{440}\left[\nabla^2 w^{(i)}(x', y') + \gamma\frac{\partial w^{(i)}(x', y')}{\partial x'}\right]\right. \\ & \left. + e_{150}\left[\nabla^2\phi^{(i)}(x', y') + \gamma\frac{\partial \phi^{(i)}(x', y')}{\partial x'}\right]\right\}dx'dy' \\ & - \int_{-l}^{l}\alpha(|x' - x|, 0)\left[\sigma_{yz}^{(1)}(x, 0^+) - \sigma_{yz}^{(2)}(x, 0^-)\right]dx' = 0 \end{aligned} \tag{18}$$

$$\begin{aligned} & e^{\gamma x}\iint_V \alpha(|x' - x|, |y' - y|)\left\{e_{150}\left[\nabla^2 w^{(i)}(x', y') + \gamma\frac{\partial w^{(i)}(x', y')}{\partial x'}\right]\right. \\ & \left. - \varepsilon_{110}\left[\nabla^2\phi^{(i)}(x', y') + \gamma\frac{\partial \phi^{(i)}(x', y')}{\partial x'}\right]\right\}dx'dy' \\ & - \int_{-l}^{l}\alpha(|x' - x|, 0)\left[D_y^{c(1)}(x, 0^+) - D_y^{c(2)}(x, 0^-)\right]dx' = 0 \end{aligned} \tag{19}$$

$\nabla^2 = \partial^2/\partial x^2 + \partial^2/\partial y^2$ is the two-dimensional Laplace operator. Here the surface integral may be dropped since the displacement and the electric displacement fields vanish at infinity.

As mentioned in [29], it can be obtained that $[\sigma_{yz}^{(1)}(x, 0^+) - \sigma_{yz}^{(2)}(x, 0^-)] = 0$ and $[D_y^{c(1)}(x, 0^+) - D_y^{c(2)}(x, 0^-)] = 0$. Hence the line integrals in Equations (18)–(19) vanish.

So it can be shown that the general solution of Equations (18)–(19) are identical to that of

$$c_{440}\left[\nabla^2 w^{(i)}(x',y') + \gamma\frac{\partial w^{(i)}(x',y')}{\partial x'}\right] + e_{150}\left[\nabla^2 \phi^{(i)}(x',y') + \gamma\frac{\partial \phi^{(i)}(x',y')}{\partial x'}\right] = 0 \quad (20)$$

$$e_{150}\left[\nabla^2 w^{(i)}(x',y') + \gamma\frac{\partial w^{(i)}(x',y')}{\partial x'}\right] - \varepsilon_{110}\left[\nabla^2 \phi^{(i)}(x',y') + \gamma\frac{\partial \phi^{(i)}(x',y')}{\partial x'}\right] = 0 \quad (21)$$

almost everywhere.

The general solutions of Equations (20)–(21) satisfying condition (4) are, respectively:

$$\begin{cases} w^{(1)}(x,y) = \dfrac{1}{2\pi}\displaystyle\int_{-\infty}^{\infty} A_1(s)e^{-\lambda y}e^{isx}ds \\ \phi^{(1)}(x,y) = \dfrac{e_{150}}{\varepsilon_{110}}w^{(1)}(x,y) + \dfrac{1}{2\pi}\displaystyle\int_{-\infty}^{\infty} B_1(s)e^{-\lambda y}e^{isx}ds \end{cases}, y \geq 0 \quad (22)$$

$$\begin{cases} w^{(2)}(x,y) = \dfrac{1}{2\pi}\displaystyle\int_{-\infty}^{\infty} A_2(s)e^{\lambda y}e^{isx}ds \\ \phi^{(2)}(x,y) = \dfrac{e_{150}}{\varepsilon_{110}}w^{(2)}(x,y) + \dfrac{1}{2\pi}\displaystyle\int_{-\infty}^{\infty} B_2(s)e^{\lambda y}e^{isx}ds \end{cases}, y \leq 0 \quad (23)$$

where $A_1(s)$, $B_1(s)$, $A_2(s)$, $B_2(s)$ are to be determined from the boundary conditions.

$$\lambda = \sqrt{s^2 - is\gamma}.$$

Substituting Equations (22)–(23) into Equations (16)–(17), it can be obtained

$$\begin{cases} \sigma_{yz}^{(1)}(x,y) = -\dfrac{e^{\gamma x}}{2\pi}\displaystyle\int_{-\infty}^{\infty}\lambda[\mu_0 A_1(s) + e_{150}B_1(s)]e^{-\lambda y}e^{isx}ds \\ D_y^{c(1)}(x,y) = \dfrac{\varepsilon_{110}e^{\gamma x}}{2\pi}\displaystyle\int_{-\infty}^{\infty}\lambda B_1(s)e^{-\lambda y}e^{isx}ds \end{cases} \quad (24)$$

$$\begin{cases} \sigma_{xz}^{(1)}(x,y) = \dfrac{ie^{\gamma x}}{2\pi}\displaystyle\int_{-\infty}^{\infty} s[\mu_0 A_1(s) + e_{150}B_1(s)]e^{-\lambda y}e^{isx}ds \\ D_x^{c(1)}(x,y) = -\dfrac{i\varepsilon_{110}e^{\gamma x}}{2\pi}\displaystyle\int_{-\infty}^{\infty} sB_1(s)e^{-\lambda y}e^{isx}ds \end{cases} \quad (25)$$

$$\begin{cases} \sigma_{yz}^{(2)}(x,y) = \dfrac{e^{\gamma x}}{2\pi}\displaystyle\int_{-\infty}^{\infty}\lambda[\mu_0 A_2(s) + e_{150}B_2(s)]e^{\lambda y}e^{isx}ds \\ D_y^{c(2)}(x,y) = -\dfrac{\varepsilon_{110}e^{\gamma x}}{2\pi}\displaystyle\int_{-\infty}^{\infty}\lambda B_2(s)e^{\lambda y}e^{isx}ds \end{cases} \quad (26)$$

$$\begin{cases} \sigma_{xz}^{(2)}(x,y) = \dfrac{ie^{\gamma x}}{2\pi}\displaystyle\int_{-\infty}^{\infty} s[\mu_0 A_2(s) + e_{150}B_2(s)]e^{\lambda y}e^{isx}ds \\ D_x^{c(2)}(x,y) = -\dfrac{i\varepsilon_{110}e^{\gamma x}}{2\pi}\displaystyle\int_{-\infty}^{\infty} sB_2(s)e^{\lambda y}e^{isx}ds \end{cases} \quad (27)$$

where $\mu_0 = c_{440} + e_{150}^2/\varepsilon_{110}$.

According to the boundary conditions (1)–(3), it can be obtained that $\sigma_{yz}^{(1)}(x,0^+) = \sigma_{yz}^{(2)}(x,0^-)$ and $D_y^{c\,(1)}(x,0^+) = D_y^{c\,(2)}(x,0^-)$. So we have

$$-\mu_0[A_1(s)+A_2(s)] - e_{150}[B_1(s)+B_2(s)] = 0 \tag{28}$$

$$B_1(s) + B_2(s) = 0 \tag{29}$$

To solve the problem, the jump of the displacement across the crack surfaces is defined as follows:

$$f(x) = w^{(1)}(x,0^+) - w^{(2)}(x,0^-) \tag{30}$$

Substituting Equations (22)–(23) into Equation (30), applying the boundary condition (3) and the Fourier transform, it can be obtained

$$\overline{f}(s) = A_1(s) - A_2(s) \tag{31}$$

$$\frac{e_{150}}{\varepsilon_{110}}[A_1(s) - A_2(s)] + B_1(s) - B_2(s) = 0 \tag{32}$$

By solving four Equations (28)–(29) and (31)–(32) with four unknown functions, it can be obtained that

$$B_1(s) = -B_2(s),\ A_1(s) = -A_2(s),\ B_1(s) = -\frac{e_{150}}{\varepsilon_{110}}A_1(s),\ A_1(s) = \overline{f}(s)/2 \tag{33}$$

Substituting Equations (24)–(27) into Equations (14)–(15) and applying α from Equation (10), it can be obtained

$$\begin{cases} \tau_{yz}^{(1)}(x,y) = -\dfrac{c_{440}}{4\pi}\displaystyle\int_{-\infty}^{\infty}\lambda\overline{f}(s)ds\int_0^{\infty}e^{-\lambda y'}dy'\int_{-\infty}^{\infty}[\alpha(|x'-x|,|y'-y|)+\alpha(|x'-x|,|y'+y|)]e^{\gamma x'}e^{isx'}dx' \\ D_y^{(1)}(x,y) = -\dfrac{e_{150}}{4\pi}\displaystyle\int_{-\infty}^{\infty}\lambda\overline{f}(s)ds\int_0^{\infty}e^{-\lambda y'}dy'\int_{-\infty}^{\infty}[\alpha(|x'-x|,|y'-y|)+\alpha(|x'-x|,|y'+y|)]e^{\gamma x'}e^{isx'}dx' \end{cases} \tag{34}$$

$$\begin{cases} \tau_{xz}^{(1)}(x,y) = -\dfrac{ic_{440}}{4\pi}\displaystyle\int_{-\infty}^{\infty}s\overline{f}(s)ds\int_0^{\infty}e^{-\lambda y'}dy'\int_{-\infty}^{\infty}[\alpha(|x'-x|,|y'-y|)+\alpha(|x'-x|,|y'+y|)]e^{\gamma x'}e^{isx'}dx' \\ D_x^{(1)}(x,y) = -\dfrac{ie_{150}}{4\pi}\displaystyle\int_{-\infty}^{\infty}s\overline{f}(s)ds\int_0^{\infty}e^{-\lambda y'}dy'\int_{-\infty}^{\infty}[\alpha(|x'-x|,|y'-y|)+\alpha(|x'-x|,|y'+y|)]e^{\gamma x'}e^{isx'}dx' \end{cases} \tag{35}$$

For the relations [54]

$$\int_0^{\infty}e^{-px^2-vx}\sin(bx)dx = -\frac{i}{4}\sqrt{\frac{\pi}{p}}\left\{\exp\left(\frac{(v-ib)^2}{4p}\right)\left[1-\Phi\left(\frac{v-ib}{2\sqrt{p}}\right)\right] - \exp\left(\frac{(v+ib)^2}{4p}\right)\left[1-\Phi\left(\frac{v+ib}{2\sqrt{p}}\right)\right]\right\} \tag{36}$$

$$\int_0^\infty e^{-px^2-vx}\cos(bx)dx = \frac{1}{4}\sqrt{\frac{\pi}{p}}\left\{\exp\left(\frac{(v-ib)^2}{4p}\right)\left[1-\Phi\left(\frac{v-ib}{2\sqrt{p}}\right)\right]+\exp\left(\frac{(v+ib)^2}{4p}\right)\left[1-\Phi\left(\frac{v+ib}{2\sqrt{p}}\right)\right]\right\} \tag{37}$$

$$\int_0^\infty \exp\left(-py^2-\gamma y\right)dy = \frac{1}{2}(\pi/p)^{1/2}\exp\left(\gamma^2/4p\right)\left[1-\Phi\left(\gamma/2\sqrt{p}\right)\right] \tag{38}$$

$$\Phi(z) = \frac{2}{\sqrt{\pi}}\int_0^z \exp\left(-t^2\right)dt \tag{39}$$

It can be obtained

$$\begin{cases} \tau_{yz}^{(1)}(x,y) = -\dfrac{c_{440}}{4\pi}\displaystyle\int_{-\infty}^{\infty}\lambda g_1(s,y)g_2(s,y)\overline{f}(s)e^{isx}ds \\ D_y^{(1)}(x,y) = -\dfrac{e_{150}}{4\pi}\displaystyle\int_{-\infty}^{\infty}\lambda g_1(s,y)g_2(s,y)\overline{f}(s)e^{isx}ds \end{cases} \tag{40}$$

$$\begin{cases} \tau_{xz}^{(1)}(x,y) = \dfrac{ic_{440}}{4\pi}\displaystyle\int_{-\infty}^{\infty}sg_1(s,y)g_2(s,y)\overline{f}(s)e^{isx}ds \\ D_x^{(1)}(x,y) = \dfrac{ie_{150}}{4\pi}\displaystyle\int_{-\infty}^{\infty}sg_1(s,y)g_2(s,y)\overline{f}(s)e^{isx}ds \end{cases} \tag{41}$$

where $g_1(s,y) = \frac{1}{2}e^{-py^2}\left\{e^{\frac{(\lambda-2py)^2}{4p}}\left[1-\Phi\left(\frac{\lambda-2py}{2\sqrt{p}}\right)\right]+e^{\frac{(\lambda+2py)^2}{4p}}\left[1-\Phi\left(\frac{\lambda+2py}{2\sqrt{p}}\right)\right]\right\}$, $g_2(s,y) = \frac{1}{2}e^{\gamma x}\left\{e^{\frac{(-\gamma-is)^2}{4p}}\left[1-\Phi\left(\frac{-\gamma-is}{2\sqrt{p}}\right)\right]+e^{\frac{(\gamma+is)^2}{4p}}\left[1-\Phi\left(\frac{\gamma+is}{2\sqrt{p}}\right)\right]\right\}$ $p = \left(\frac{\beta}{a}\right)^2$. So the boundary conditions (1) and (3) can be expressed as:

$$\tau_{yz}^{(1)}(x,0) = -\frac{c_{440}\,e^{\gamma x}}{4\pi}\int_{-\infty}^{\infty}\lambda g_0(s)\overline{f}(s)e^{isx}ds = -\tau_0(x),\ -l \le x \le l \tag{42}$$

$$\int_{-\infty}^{\infty}\overline{f}(s)e^{isx}ds = 0,\ |x| > l \tag{43}$$

Where $g_0(s) = \frac{1}{2}e^{\frac{\lambda^2+(\gamma+is)^2}{4p}}\left[1-\Phi\left(\frac{\lambda}{2\sqrt{p}}\right)\right]\left[2-\Phi\left(\frac{-\gamma-is}{2\sqrt{p}}\right)-\Phi\left(\frac{\gamma+is}{2\sqrt{p}}\right)\right]$
$= e^{\frac{\gamma^2+is\gamma}{4p}}\left[1-\Phi\left(\frac{\lambda}{2\sqrt{p}}\right)\right]$, $\Phi(z) = -\Phi(-z)$.

It can be obtained that $\lim_{a\to 0} g_0(s) = 1$. So Equations (42)–(43) will revert to the well-known dual integral equations for the same problem in the classical theory for the limit $a \to 0$. To determine the unknown function $\overline{f}(s)$, the dual integral equations (42) and (43) must be solved.

5 Solution of the Dual Integral Equations

The only difference between the classical and non-local equations is in the function $g_0(s)$, it is logical to utilize the classical solution to convert the system Equations (42)–(43) to an integral equation of the second kind, which is generally better behaved. For the lattice parameter $a \to 0$, then $g_0(s)$ equals to a non-zero constant and Equations (42)–(43) reduce to a pair of dual integral equations for the same problem in classical piezoelectric materials. As discussed in [29], the dual integral Equations (42)–(43) cannot be transformed into a

Fredholm integral equation of the second kind, because $g_0(s)$ does not tend to a constant $C(C \neq 0)$ for $s \to \infty$. Of course, the dual integral Equations (42)–(43) can be considered to be a single integral equation of the first kind with discontinuous kernel. It is well-known in the literature that integral equations of the first kind are generally ill-posed in sense of Hadamard, i.e., small perturbations of the data can yield arbitrarily large changes in the solution. This makes the numerical solution of such equations quite difficult. To overcome the difficult, the Schmidt method [51] is used to solve the dual integral Equations (42)–(43). The displacement jumps across the crack surface can be represented by the following series:

$$f(x) = w^{(1)}(x, 0^+) - w^{(2)}(x, 0^-) = \sum_{n=0}^{\infty} a_n P_n^{\left(\frac{1}{2},\frac{1}{2}\right)}\left(\frac{x}{l}\right)\left(1 - \frac{x^2}{l^2}\right)^{\frac{1}{2}}, \text{ for } -l \le x \le l \quad (44)$$

$$f(x) = w^{(1)}(x, 0^+) - w^{(2)}(x, 0^-) = 0, \text{ for } |x| > l \quad (45)$$

where a_n is unknown coefficients to be determined and $P_n^{\left(1/2,1/2\right)}(x)$ is a Jacobi polynomial [54]. The Fourier transformation [55] of Equations (44)–(45) are

$$\overline{f}(s) = \sum_{n=0}^{\infty} a_n G_n \frac{1}{s} J_{n+1}(sl),\ G_n = 2\sqrt{\pi}(-1)^n i^n \frac{\Gamma\left(n + 1 + \frac{1}{2}\right)}{n!} \quad (46)$$

where $\Gamma(x)$ and $J_n(x)$ are the Gamma and Bessel functions, respectively.

Substituting Equation (46) into Equations (42)–(43), respectively, Equation (43) can be automatically satisfied. Then the remaining Equation (42) reduces to the form,

$$\frac{c_{440}e^{\gamma x}}{4\pi} \sum_{n=0}^{\infty} a_n G_n \int_{-\infty}^{\infty} \frac{\lambda}{s} g_0(s) J_{n+1}(sl) e^{isx} ds = \tau_0(x),\ -l \le x \le l \quad (47)$$

For a large s, the integrands of Equation (47) are almost decreases exponentially. So they can be evaluated numerically. Equation (47) can now be solved for the coefficients a_n by the Schmidt method [51]. It can be seen in [45–48]. Here, it was omitted.

6 Numerical Calculations and Discussion

From the works in [45–48], it can be seen that the Schmidt method is performed satisfactorily if the first 10 terms of infinite series to Equation (47) are retained. The coefficients a_n are known, so that entire stress and the electric displacement fields can be obtained. However, in fracture mechanics, it is of importance to determine the perturbation stress $\tau_{yz}^{(1)}$ and $\tau_{xz}^{(1)}$, the perturbation electric displacement $D_y^{(1)}$ and $D_x^{(1)}$ in the vicinity of the crack tips. Since the volume energy density function that was proposed by Sih and Zuo [7, 8] and in [56–58] can be as a fracture criterion for the piezoelectric materials in contrast to the idea of Griffith's energy release rate, the volume energy density function $\frac{dW}{dV}$ near the crack tips was also examined in the present paper. In the case of the present study, $\tau_{yz}^{(1)}$, $D_y^{(1)}$, $\tau_{xz}^{(1)}$, $D_x^{(1)}$ and $\frac{dW}{dV}$ can be expressed, respectively, as

$$\begin{cases} \tau_{yz} = \tau_{yz}^{(1)}(x, 0) = \dfrac{-c_{440}e^{\gamma x}}{4\pi} \displaystyle\sum_{n=0}^{\infty} a_n G_n \int_{-\infty}^{\infty} \frac{\lambda}{s} g_0(s) J_{n+1}(sl) e^{isx} ds \\ D_y = D_y^{(1)}(x, 0) = -\dfrac{e_{150}e^{\gamma x}}{4\pi} \displaystyle\sum_{n=0}^{\infty} a_n G_n \int_{-\infty}^{\infty} \frac{\lambda}{s} g_0(s) J_{n+1}(sl) e^{isx} ds = \dfrac{e_{150}}{c_{440}} \tau_{yz}^{(1)}(x, 0) \end{cases} \quad (48)$$

$$\begin{cases} \tau_{xz} = \tau_{xz}^{(1)}(x,0) = \dfrac{ic_{440}e^{\gamma x}}{4\pi}\displaystyle\sum_{n=0}^{\infty} a_n G_n \int_{-\infty}^{\infty} g_0(s) J_{n+1}(sl) e^{isx} ds \\ D_x = D_x^{(1)}(x,0) = \dfrac{e_{150}e^{\gamma x}}{4\pi}\displaystyle\sum_{n=0}^{\infty} a_n G_n \int_{-\infty}^{\infty} g_0(s) J_{n+1}(sl) e^{isx} ds = \dfrac{e_{150}}{c_{440}}\tau_{xz}^{(1)}(x,0) \end{cases} \tag{49}$$

$$\frac{dW(r,\theta)}{dV} = \frac{dW(x,y)}{dV} = \frac{1}{2}\tau_{xz}^{(1)}\frac{\partial w^{(1)}}{\partial x} + \frac{1}{2}\tau_{yz}^{(1)}\frac{\partial w^{(1)}}{\partial y} + \frac{1}{2}D_x^{(1)}E_x^{(1)} + \frac{1}{2}D_y^{(1)}E_y^{(1)} \tag{50}$$

where $x = l + r\cos\theta°$, $y = r\sin\theta°$ (r is the polar radius and $\theta°$ is the polar angle as shown in Figure 1. $0° \le \theta° \le 90°$ for the crack right tip. $90° \le \theta° \le 180°$ for the crack left tip). $E_x^{(1)}$ and $E_y^{(1)}$ are the electric field intensity, i.e., $E_x^{(1)} = -\frac{\partial\phi^{(1)}}{\partial x}$, $E_y^{(1)} = -\frac{\partial\phi^{(1)}}{\partial y}$.

So long as $a/\beta \neq 0$, the semi-infinite integration and the series in Equations (48)–(49) are convergent for any variable x. Equations (48)–(49) give finite stress and electric displacement all along $y = 0$, so there is no stress and electric displacement singularities at the crack tips. However, for $a/\beta = 0$, we have the classical stress and electric displacement singularities at the crack tips. At $-l < x < l$, $\tau_{yz}^{(1)}/.\tau_0$ is very close to negative unity, and for $x > l$ or $x < -l$, $\tau_{yz}^{(1)}\Big/\tau_0$ possesses finite values diminishing from a finite value at $x = \pm l$ to zero at $x = \pm\infty$. This is also proved that the Schmidt method can be used to solve the present problem. In all computations, the piezoelectric material is assumed to be the commercially available piezoelectric PZT-4. The material constants of PZT-4 are $c_{440} = 2.56$ ($\times 10^{10}$ N/m^2), $e_{150} = 12.7(\mathrm{c/m^2})$ and $\varepsilon_{110} = 64.6$ ($\times 10^{-10}$ $\mathrm{c/Vm^2}$), respectively. The crack surface loading $-\tau_0(x)$ will simply be assumed to be a polynomial of the form as follows:

$$-\tau_0(x) = -p_0 - p_1\left(\frac{x}{l}\right) - p_2\left(\frac{x}{l}\right)^2 - p_3\left(\frac{x}{l}\right)^3 \tag{51}$$

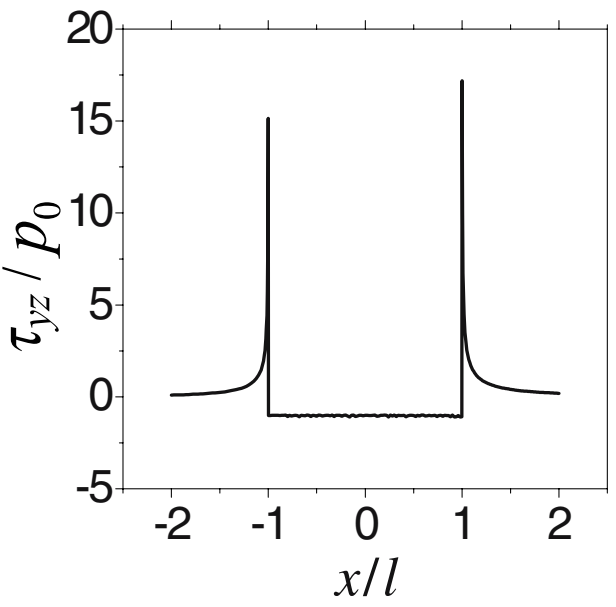

Figure 2 The stress along the crack line *versus* x/l for $l = 1.0$, $\gamma l = 0.4$ and $a/\beta l = 0.001$ under the loading $\tau_0(x) = p_0$

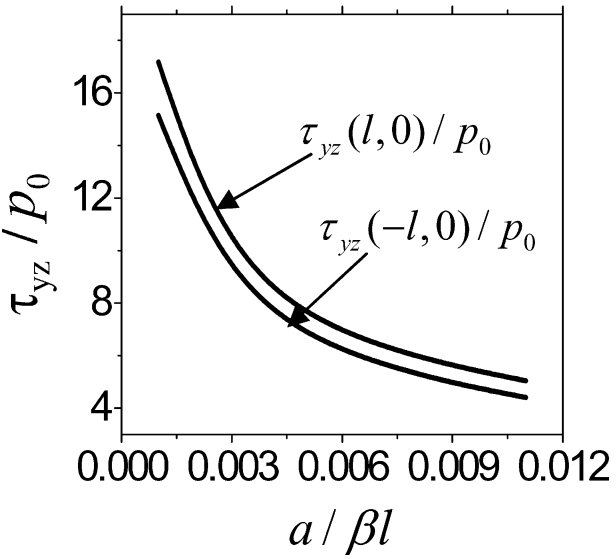

Figure 3 The stress at the crack tips *versus* $a/\beta l$ for $l = 1.0$ and $\gamma l = 0.4$ under the loading $\tau_0(x) = p_0$

Since the problem is linear, the results can be superimposed in any suitable manner. The results are obtained by taking only one of the four input parameters P_0, P_1, P_2 and P_3 nonzero at a time. The normalized non-homogeneity constant γl is varied between −2.0 and 2.0, which covers most of the practical cases.

The results of the stress and the electric displacement fields are plotted in Figure 2 to Figure 19. The following observations are very significant:

(a) The material variation direction of FGPMs in the present paper is parallel to x-axis and it is a non-symmetrical fracture problem. However, the material variation direction of

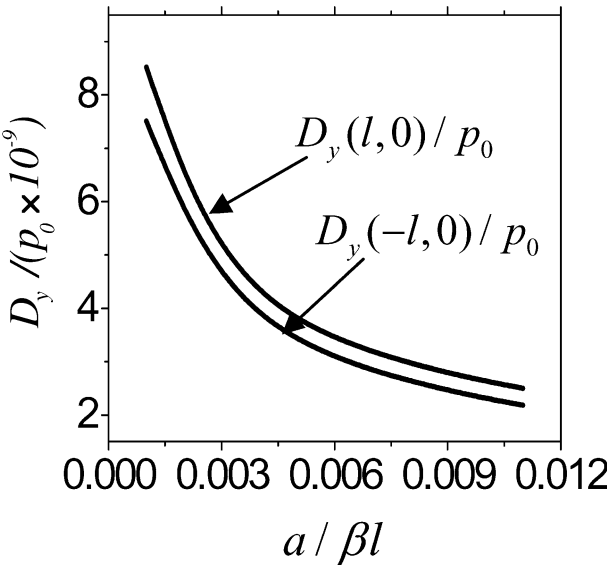

Figure 4 The electric displacement at the crack tips *versus* $a/\beta l$ for $l = 1.0$ and $\gamma l = 0.4$ under the loading $\tau_0(x) = p_0$

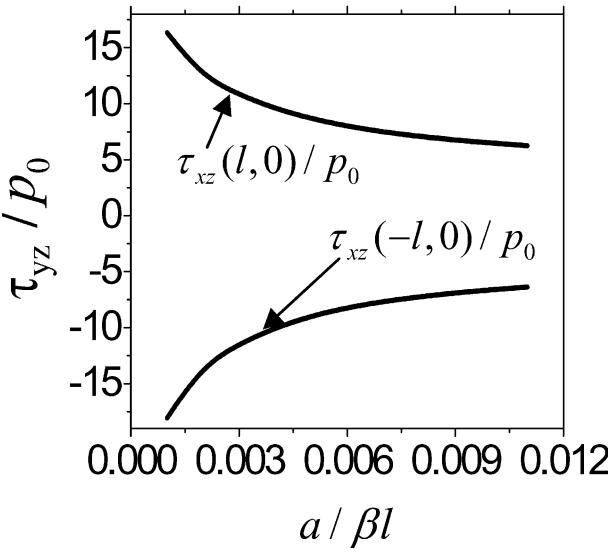

Figure 5 The stress at the crack tips *versus* $a/\beta l$ for $l = 1.0$ and $\gamma l = 0.4$ under the loading $\tau_0(x) = p_0$

FGPMs in another previous paper [50] is vertical to *y*-axis and it is a symmetrical fracture problem. This is the primary different between the present paper and the previous paper [50]. Other, the form of the loading in the present paper is more complex than one in the previous paper [50].

(b) The traditional concepts of the non-local theory are extended to solve the fracture problem of functionally graded piezoelectric materials. Here, we just attempt to give a theoretical solution for this problem. It can be found that the stress and electric displacement fields in the functionally graded piezoelectric materials carry the same

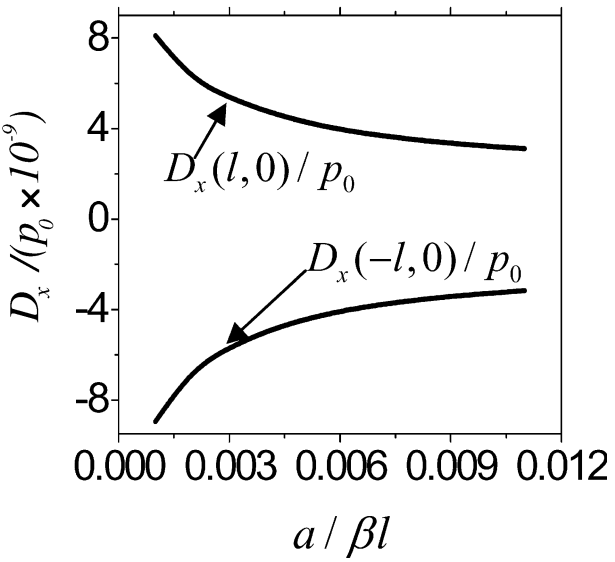

Figure 6 The electric displacement at the crack tips *versus* $a/\beta l$ for $l = 1.0$ and $\gamma l = 0.4$ under the loading $\tau_0(x) = p_0$

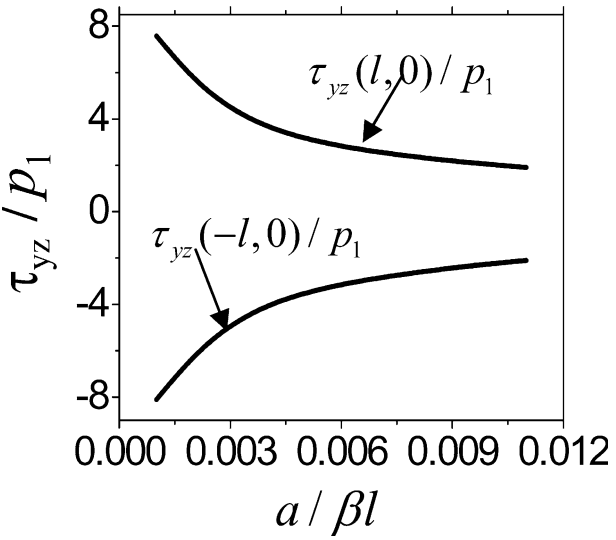

Figure 7 The stress at crack tips *versus* $a/\beta l$ for $l = 1.0$ and $\gamma l = 0.4$ under the loading $\tau_0(x) = p_1 x/l$

forms as those in a homogeneous piezoelectric materials [44] but the magnitudes of the stress and electric displacement fields are dependent on the gradient of the functionally graded piezoelectric material properties. When $\gamma = 0$, the present problem will revert to the same problem as discussed in [44]. The results of the present paper are the same as ones in [44] as shown in Figure 10 for $\gamma = 0$.

(c) For $a/\beta \neq 0$, it can be proved that the semi-infinite integrations and the series in Equations (48)–(49) are convergent for any variable x. So the stress and the electric displacement fields give finite values all along the crack line. Contrary to the classical piezoelectric theory solution, it is found that no stress and electric displacement singu-

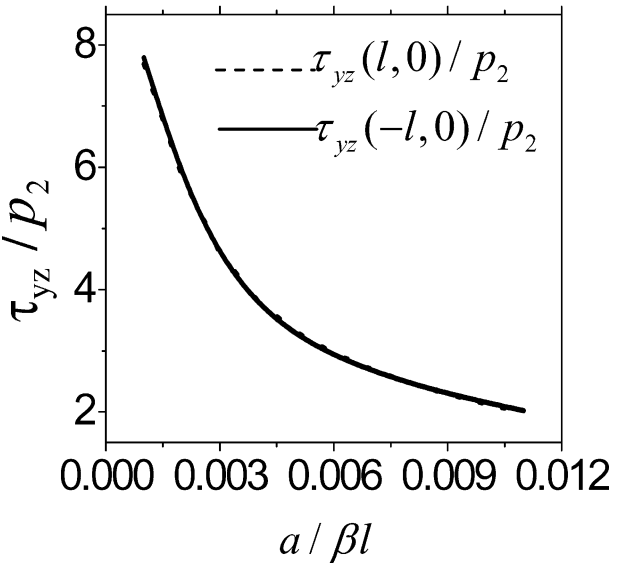

Figure 8 The stress along the crack line *versus* $a/\beta l$ for $l = 1.0$ and $\gamma l = 0.4$ under the loading $\tau_0(x) = p_2(x/l)^2$

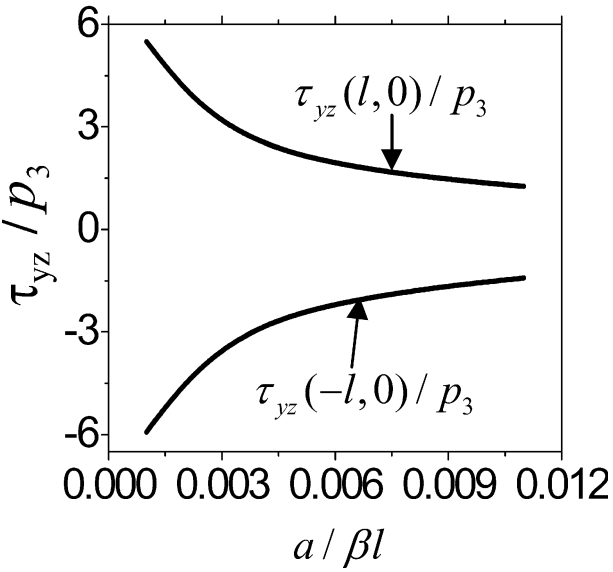

Figure 9 The stress along the crack line *versus* $a/\beta l$ for $l = 1.0$ and $\gamma l = 0.4$ under the loading $\tau_0(x) = p_3(x/l)^3$

larities are present at the crack tips, and also the present results converge to the classical ones when far away from the crack tips as shown in Figure 2.

(d) The stresses at the crack tips become infinite as the atomic distance $a \to 0$.This is the classical continuum limit of square root singularity. This can be shown from Equations (42)–(43). For $a \to 0$, $g_0(s) = 1$, Equations (42)–(43) will reduce to the dual integral equations for the same problem in classical functionally graded piezoelectric materials as shown in [15]. These dual integral equations can be solved by using the singular integral equation for the same problem as in the local functionally graded piezoelectric materials

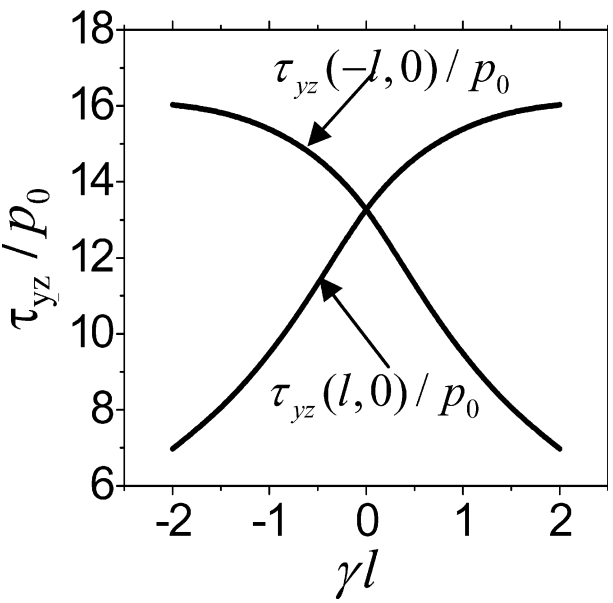

Figure 10 The stress at crack tips *versus* γl for $l = 1.0$ and $a/\beta l = 0.002$ under the loading $\tau_0(x) = p_0$

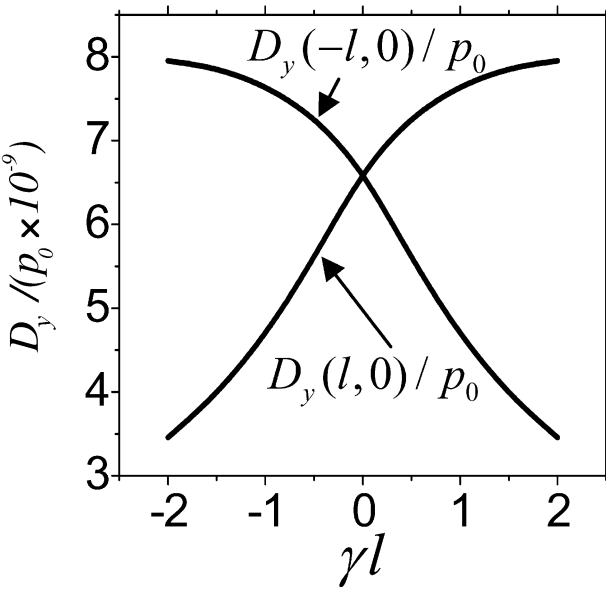

Figure 11 The electric displacement at crack tips *versus* γl for $l = 1.0$ and $a/\beta l = 0.002$ under the loading $\tau_0(x) = p_0$

problem. However, the stress and the electric displacement singularities are present at the crack tips in the local functionally graded piezoelectric materials problem as well known.

(e) As shown in Equations (47)–(49), it can be obtained that the dimensionless stress fields $\tau_{yz}^{(1)}$ and $\tau_{xz}^{(1)}$ are found to be independent of the material parameters c_{440}. They just depend on the length of the crack, the functionally graded parameter and the lattice parameter. This is the same as the anti-plane shear fracture problem in the homogeneous piezoelectric materials. However, the electric displacement fields $D_y^{(1)}$

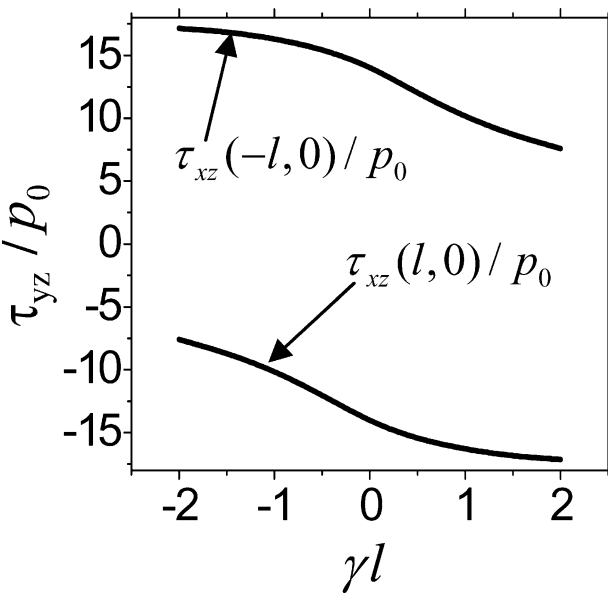

Figure 12 The stress at the crack tips *versus* γl for $l = 1.0$ and $a/\beta l = 0.002$ under the loading $\tau_0(x) = p_0$

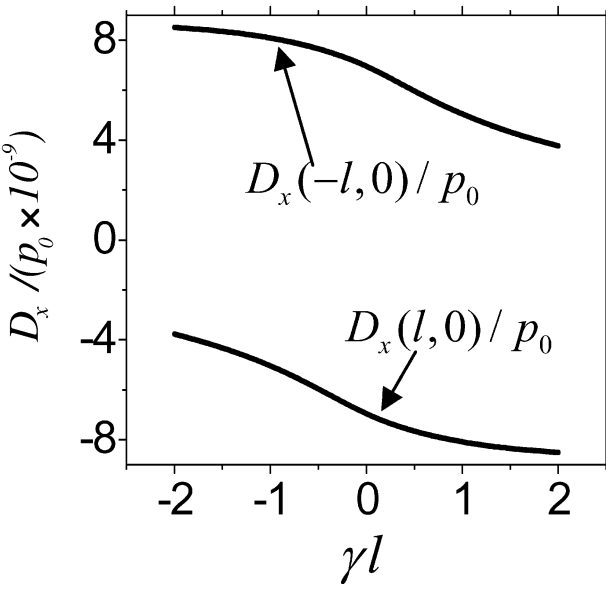

Figure 13 The electric displacement at crack tips *versus* γl for $l = 1.0$ and $a/\beta l = 0.002$ under the loading $\tau_0(x) = p_0$

and $D_x^{(1)}$ are found to depend on the stress loads, the material parameter c_{440}, the length of the crack, the functionally graded parameter, the dielectric parameter and the lattice parameter as shown in Equations (48)–(49). The relations between the electric displacement fields and the stress fields near the crack tips can be obtained as shown in Equations (48)–(49). However, the amplitude values of the electric displacement field and the stress field are different from each other. The amplitude values of the electric displacement fields are very small as shown in Figures 4, 6, 11 and 13.

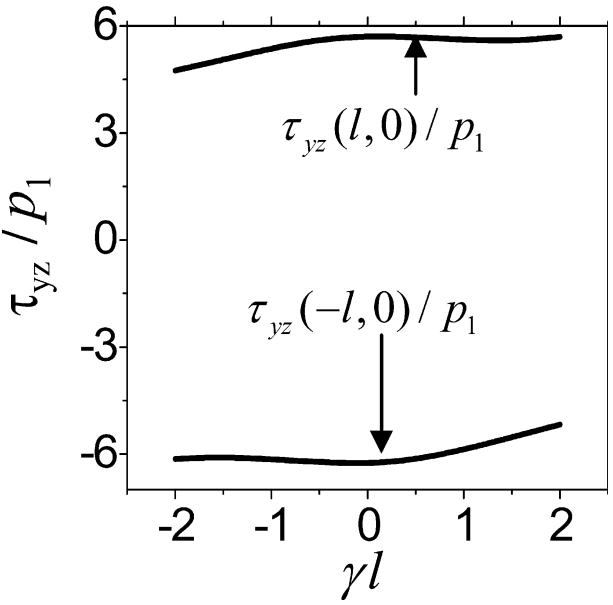

Figure 14 The stress along the crack line *versus* γl for $l = 1.0$ and $a/\beta l = 0.002$ under the loading $\tau_0(x) = p_1 x/l$

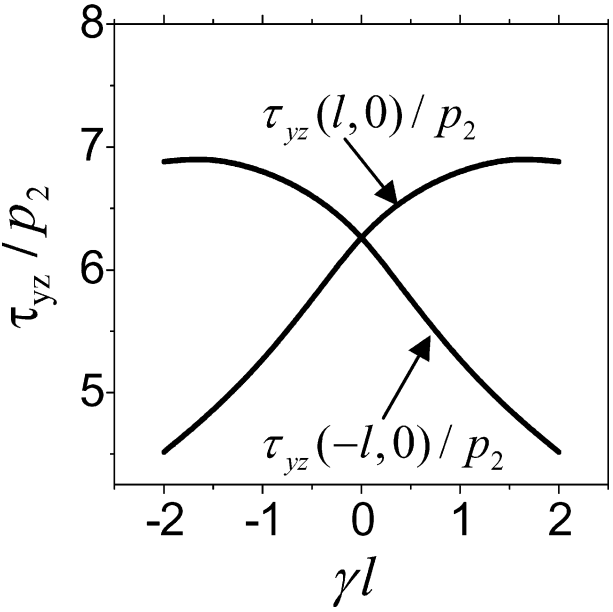

Figure 15 The stress along the crack line *versus* γl for $l = 1.0$ and $a/\beta l = 0.002$ under the loading $\tau_0(x) = p_2(x/l)^2$

(f) For the symmetric loading, the effect of the lattice parameter of the functionally graded materials on the stress field τ_{yz} and the electric displacement field D_y at the crack tips decrease with increase of the lattice parameter as shown in as shown in Figures 3, 4 and 8. However, as shown in Figures 5 and 6 for the symmetric loading, the effect of the lattice parameter of the functionally graded materials on the stress field τ_{xz} and the electric displacement field D_x at the crack right tip decrease with increase of the lattice parameter. The absolute values of the stress field τ_{xz} and the electric displacement field D_x at the crack left tip decrease with increase of the lattice

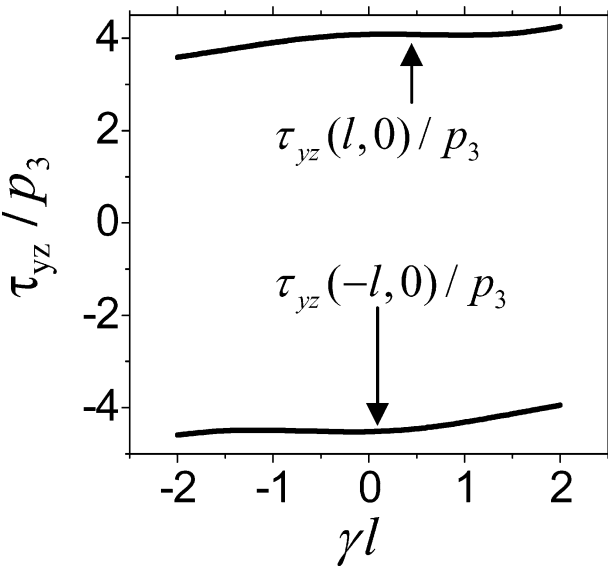

Figure 16 The stress along the crack line *versus* γl for $l = 1.0$ and $a/\beta l = 0.002$ under the loading $\tau_0(x) = p_3(x/l)^3$

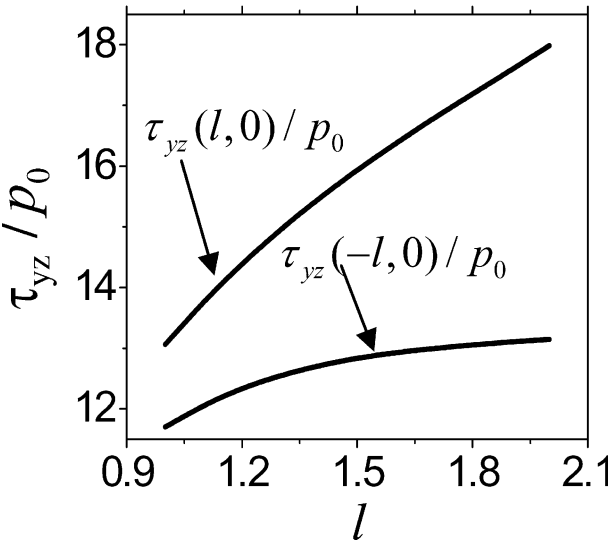

Figure 17 The stress at the crack tip *versus* l for $\lambda l = 0.4$ and $a/\beta l = 0.002$ under the loading $\tau_0(x) = p_0$

parameter. The change tendencies of these stress fields τ_{xz} at the crack left tip and at the crack right tip are almost opposite as shown in Figure 5. The electric displacement fields D_x at the crack left tip and at the crack right tip are also opposite as shown in Figure 6. For the anti-symmetric loading, as shown in Figures 7 and 9, the effect of the lattice parameter of the functionally graded materials on the stress field τ_{yz} at the crack right tip decreases with increase of the lattice parameter. However, the absolute value of the stress field τ_{yz} at the crack left tip decreases with increase of the lattice parameter. Simultaneously, for the non-local solution, the smaller the lattice parameter is, the closer to the classical solution.

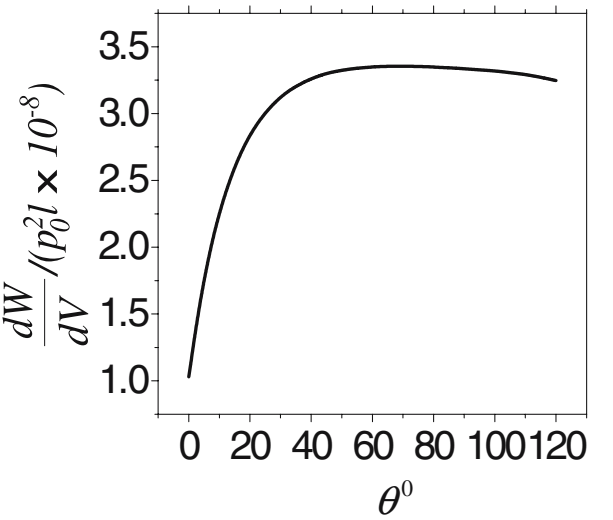

Figure 18 The volume energy density function $\frac{dW}{dV}$ near the crack right tip versus θ^0 for $l = 1.0$, $r/l = 0.001$, $\gamma l = 0.4$ and $a/\beta l = 0.002$ under the loading $\tau_0(x) = p_0$

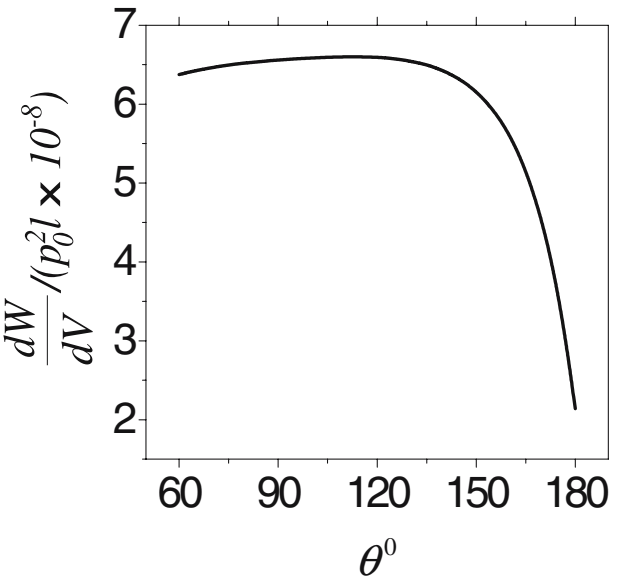

Figure 19 The volume energy density function $\frac{dW}{dV}$ near the crack left tip versus θ^0 for $l = 1.0$, $r/l = 0.001$, $\gamma l = 0.4$ and $a/\beta l = 0.002$ under the loading $\tau_\theta(x) = p_0$

(g) For the symmetric loading, as shown in Figures 10, 11 and 15, the value of the stress field τ_{yz} and the electric displacement field D_y at crack left tip decreases with increase of γl. However, the value of the stress field τ_{yz} and the electric displacement field D_y at crack left tip increases with increase of γl. The change tendencies of these stress fields τ_{yz} and the electric displacement fields D_y at the crack left tip and at the crack right tip are quite opposite, respectively. However, as shown in Figures 12 and 13, for the symmetric loading, the stress field τ_{xz} and the electric displacement field D_x at the crack tips decrease with increase of γl. For the anti-symmetric loading, as shown in Figures 14 and 16, the value of the stress field at crack left tip is a negative value. However, the value of the stress field at crack right tip is a positive value. They are almost symmetric about the line $\tau_{yz} = 0$. When $\gamma = 0$, the present problem will revert to the same problem as ones in [44]. The results of the present paper are the same as ones in [44] as shown in Figures 10 and 15. Certainly, the solving process of the present paper is similar with ones of [47–50]. However, the material properties and the basic equations of the present paper are more complex than ones of [47–50].

(h) The values of the stress fields at the crack tips almost linearly increase with increase of the crack length as shown in Figure 17. This is similar with results of the classical theory. For the classical theory, the stress intensity factors linearly increase with increase of the crack length.

(i) For $0° \le \theta° \le 120°$, the volume energy density function $\frac{dW}{dV}$ near the crack right tip tends to increase with polar angle $\theta°$ reaches a peak and then to decrease slowly in magnitude as shown in Figure 18 to Figure 19. The maximum value of $\frac{dW}{dV}$ is found to occur at about $\theta° = 60°$ near the crack right tip. For $60° \le \theta° \le 180°$ the volume energy density function $\frac{dW}{dV}$ near the crack left tip tends to increase slowly with polar angle $\theta°$ reaches a peak and then to decrease in magnitude as shown in Figure 18 to Figure 19. The maximum value of $\frac{dW}{dV}$ is found to occur at about $\theta° = 120°$ near the crack left tip. As discussed in [7, 8], these can be used to predict the bifurcate direction of the crack growth under electric and mechanical combined mixed mode conditions.

7 Conclusion

In the present paper, the traditional concepts of the non-local theory are firstly extended to solve the fracture problem of functionally graded piezoelectric materials. As expected, the solution of the present paper does not contain the stress and the electric displacement singularities at the crack tips. It can be obtained that the solution of the present paper yields *a finite stress* at the crack tips, thus allows us to use the maximum stress as a fracture criterion. On the other hand, the properties of the volume energy density functions near the crack tips have been also studied. These results can be used to predict the bifurcate direction of the crack growth under electric and mechanical combined mixed mode conditions.

Acknowledgements The authors are grateful for the financial support by the National Natural Science Foundation of China (10572043, 10572155), the Natural Science Foundation with Excellent Young Investigators of Hei Long Jiang Province (JC04-08).

References

1. Beom, H.G., Atluri, S.N.: Near-tip fields and intensity factors for interfacial cracks in dissimilar anisotropic piezoelectric media. Int. J. Fract. **75**(2), 163–183 (1996)
2. Gao, H.J., Zhang, T.Y., Tong, P.: Local and global energy rates for an elastically yielded crack in piezoelectric ceramics. J. Mech. Phys. Solids **45**(2), 491–510 (1997)
3. Han, X.L., Wang, T.: Interacting multiple cracks in piezoelectric materials. Int. J. Solids Struct. **36**(27), 4183–4202 (1999)
4. Narita, K., Shindo, Y., Watanabe, K.: Anti-plane shear crack in a piezoelectric layered to dissimilar half spaces. JSME Int. J. Ser. A **42**(1), 66–72 (1999)
5. Yu, S.W., Chen, Z.T.: Transient response of a cracked infinite piezoelectric strip under anti-plane impact. Fatigue Eng. Mater. Struct. **21**, 1381–1388 (1998)
6. Zhang, T.Y., Hack, J.E.: Mode-III cracks in piezoelectric materials. J. Appl. Physi. **71**, 5865–5870 (1992)
7. Zuo, J.Z., Sih, G.C.: Energy density formulation and interpretation of cracking behavior for piezoelectric ceramics. Theor. Appl. Fract. Mech. **34**(1), 17–33 (2000)
8. Sih, G.C., Zuo, J.Z.: Energy density formulation and interpretation of cracking behavior for piezoelectric ceramics. Theor. Appl. Fract. Mech. **34**(2), 123–141 (2000)
9. Takagi, K., Li, J.F., Yokoyama, S., Watanabe, R.: Fabrication and evaluation of PZT/Pt piezoelectric composites and functionally graded actuators. J. Eur. Ceram. Soc. **23**(10), 1577–1583 (2003)
10. Chue, C.H., Qu, Y.L.: Mode III crack problems for two bonded functionally graded piezoelectric materials. Int. J. Solids Struct. **42**, 3321–3337 (2005)
11. Chen, J., Liu, Z.X., Zou, Z.Z.: Electromechanical impact of a crack in a functionally graded piezoelectric medium. Theor. Appl. Fract. Mech. **39**(1), 47–60 (2003)
12. Jin, B., Zhong, Z.: A moving mode-III crack in functionally graded piezoelectric material: Permeable problem. Mech. Res. Commun. **29**(4), 217–224 (2002)
13. Wang, B.L.: A mode-III crack in functionally graded piezoelectric materials. Mech. Res. Commun. **30** (2), 151–159 (2003)
14. Kwon, S.M.: Electrical nonlinear anti-plane shear crack in a functionally graded piezoelectric strip. Int. J. Solids Struct. **40**(21), 5649–5667 (2003)
15. Li, C.Y., Weng, G.J.: Antiplane crack problem in functionally graded piezoelectric materials. J. App. Mech. **69**(4), 481–488 (2002)
16. Deeg, W.E.F.: The analysis of dislocation, crack and inclusion problems in piezoelectric solids. PhD thesis, Stanford University (1980)
17. Pak, Y.E.: Crack extension force in a piezoelectric material. J. Appl. Mech. **57**, 647–653 (1990)
18. Han, J.J., Chen, Y.H.: Multiple parallel cracks interaction problem in piezoelectric ceramics. Int. J. Solids Struct. **36**, 3375–3390 (1999)
19. Parton, V.S.: Fracture mechanics of piezoelectric materials. ACTA Astronautra **3**, 671–683 (1976)
20. Mikhailov, G.K., Parton, V.S.: Electromagnetoelasticity. Hemisphere, New York (1990)

21. Hao, T.H., Shen, Z.Y.: A new electric boundary condition of electric fracture mechanics and its applications. Eng. Fract. Mech. **47**(6), 793–802 (1994)
22. Soh, A.K., Fang, D.N., Lee, K.L.: Analysis of a bi-piezoelectric ceramic layer with an interfacial crack subjected to anti-plane shear and in-plane electric loading. Eur. J. Mech. A, Solids (19), 961–977 (2000)
23. Sosa, H.: On the fracture mechanics of piezoelectric solids. Int. J. Solids Struct. **29**, 2613–2622 (1992)
24. Zhang, T.Y., Qian, C.F., Tong, P.: Linear electro-elastic analysis of a cavity or a crack in a piezoelectric material. Int. J. Solids Struct. **35**, 2121–2149 (1998)
25. Zhong, Z., Meguid, S.A.: Analysis of a circular arc-crack in piezoelectric materials. Int. J. Fract. **84**, 143–158 (1997)
26. McMeeking, R.M.: On mechanical stress at cracks in dielectrics with application to dielectric breakdown. J. Appl. Physi. **62**, 3122–3316 (1989)
27. Rice, J.R.: A path independent integral and the approximate analysis of strain concentrations by notches and cracks. ASME J. Appl. Mech. **35**, 379–386 (1968)
28. Xia, Z.C., Hutchinson, J.W.: Crack tip fields in strain gradient plasticity. J. Mech. Phys. Solids **44**, 1621–1648 (1996)
29. Eringen, A.C., Speziale, C.G., Kim, B.S.: Crack tip problem in nonlocal elasticity. J. Mech. Phys. Solids **25**, 339–346 (1977)
30. Eringen, A.C.: Linear crack subject to shear. Int. J. Fract. **14**, 367–379 (1978)
31. Eringen, A.C.: Linear crack subject to anti-plane shear. Eng. Fract. Mech. **12**, 211–219 (1979)
32. Edelen, D.G.B.: Nonlocal field theory. In: Eringen, A.C. (ed.) Continuum Physics. Fourth Volume, pp. 75–204. New York, Academic Press (1976)
33. Green, A.E., Rivilin, R.S.: Multipolar continuum mechanics: Functional theory. I. Proc. R. Soc. Lond. A. **284**, 303–315 (1965)
34. Eringen, A.C.: Nonlocal polar field theory. In: Eringen, A.C. (ed.) Continuum Physics. Fourth Volume, pp. 205–267. Academic Press, New York (1976)
35. Pan, K.L., Takeda, N.: Nonlocal stress field of interface dislocations. Arch. Appl. Mech. **68**, 179–184 (1998)
36. Pan, K.L.: The image force on a dislocation near an elliptic hole in nonlocal elasticity. Arch. Appl. Mech. **62**, 557–564 (1992)
37. Pan, K.L.: The image force theorem for a screw dislocation near a crack in nonlocal elasticity. J. Appl. Physi. **27**, 344–346 (1994)
38. Pan, K.L.: Interaction of a dislocation with a surface crack in nonlocal elasticity. Int. J. Fract. **69**, 307–318 (1995)
39. Pan, K.L., Fang, J.: Nonlocal interaction of dislocation with a crack. Arch. Appl. Mech. **64**, 44–51 (1993)
40. Eringen, A.C., Kim, B.S.: On the problem of crack in nonlocal elasticity. In: Thoft-Christensen, P. (ed.) Continuum Mechanics Aspects of Geodynamics and Rock Fracture Mechanics, pp. 81–113. Reidel, Dordrecht, Holland (1974)
41. Eringen, A.C., Kim, B.S.: Relation between nonlocal elasticity and lattice dynamics. Cryst. Lattice Defects **7**, 51–57 (1977)
42. Zhou, Z.G., Du, S.Y., Wang, B.: Investigation of anti-plane shear behavior of a Griffith crack in a piezoelectric materials by using the non-local theory. Int. J. Fract. **111**(2), 105–117 (2001)
43. Zhou, Z.G., Wang, B.: Investigation of anti-plane shear behavior of two collinear impermeable cracks in the piezoelectric materials by using the nonlocal theory. Int. J. Solids Struct. **39**, 1731–1742 (2003)
44. Zhou, Z.G., Du, S.Y., Wang, B.: On anti-plane shear behavior of a Griffith permeable crack in piezoelectric materials by use of the non-local theory. ACTA Mech. Sin. **19**(2), 181–188 (2003)
45. Zhou, Z.G., Sun, J.L., Wang, B.: Investigation of the behavior of a crack in a piezoelectric material subjected to a uniform tension loading by use of the non-local theory. Int. J. Eng. Sci. **42**(19–20), 2041–2063 (2004)
46. Zhou, Z.G., Wang, B.: Investigation of the interaction of two collinear cracks in anisotropic elasticity materials by means of the nonlocal theory. Int. J. Eng. Sci. **43**(13–14), 1107–1120 (2005)
47. Zhou, Z.G., Han, J.C., Du, S.Y.: Investigation of a Griffith crack subject to anti-plane shear by using the non-local theory. Int. J. Solids Struct. (36), 3891–3901 (1999)
48. Zhou, Z.G., Wang, B., Du, S.Y.: Investigation of the scattering of harmonic elastic anti-plane shear waves by a finite crack using the non-local theory. Int. J. Fract. (91), 13–22 (1998)
49. Zhou, Z.G., Wang, B.: Non-local theory solution of two collinear cracks in the functionally graded materials. Int. J. Solids Struct. **43**(5), 887–898 (2006)
50. Zhou, Z.G., Du, S.Y., Wu, L.Z., Wu: Investigation of anti-plane shear behavior of a Griffith permeable crack in functionally graded piezoelectric materials by use of the non-local theory. Composite and Structures, in press (2006)
51. Morse, P.M., Feshbach, H.: Methods of Theoretical Physics, First Volume, McGraw-Hill, New York (1958)

52. Eringen, A.C.: Non-local elasticity and waves. In: Thoft-Christensen, P. (ed.) Continuum Mechanics Aspects of Geodynamics and Rock Fracture Mechanics, pp. 81–105. Dordrecht, Holland (1974)
53. Eringen, A.C.: Continuum mechanics at the atomic scale. Cryst. Lattice Defects (7), 109–130 (1977)
54. Gradshteyn, I.S., Ryzhik, I.M.: Table of Integral, Series and Products. Academic Press, New York (1980)
55. Erdelyi, A. (ed.) Tables of Integral Transforms, First Volume, McGraw-Hill, New York (1954)
56. Zhou, Z.G., Sun, Y.G., Wang, B.: Crack bifurcation predicted for dynamic anti-plane collinear cracks in piezoelectric materials using a non-local theory. Theor. Appl. Fract. Mech. **39**(2), 169–180 (2003)
57. Wang, B.L., Noda, N.: Mixed mode crack initiation in piezoelectric ceramic strip. Theor. Appl. Fract. Mech. **34**(1), 35–47 (2000)
58. Shen, S., Nishioka, T.: Fracture of piezoelectric materials: Energy density criterion. Theor. Appl. Fract. Mech. 33(1), 57–65 (2000)